Weed Science 2007 55:671–678

Estimating Yellow Starthistle (*Centaurea solstitialis*) Leaf Area Index and Aboveground Biomass with the Use of Hyperspectral Data

Shaokui Ge, Ming Xu, Gerald L. Anderson, and Raymond I. Carruthers*

Hyperspectral remote-sensed data were obtained via a Compact Airborne Spectrographic Imager-II (CASI-II) and used to estimate leaf-area index (LAI) and aboveground biomass of a highly invasive weed species, yellow starthistle (YST). In parallel, 34 ground-based field plots were used to measure aboveground biomass and LAI to develop and validate hyperspectral-based models for estimating these measures remotely. Derivatives of individual hyperspectral bands improved the correlations between imaged data and actual on-site measurements. Six derivative-based normalized difference vegetation indices (DNDVI) were developed; three of them were superior to the commonly used normalized difference vegetation index (NDVI) in estimating aboveground biomass of YST, but did not improve estimates of LAI. The locally integrated derivatives-based vegetation indices (LDVI) from adjacent bands within three different spectral regions (the blue, red, and green reflectance ranges) were used to enhance absorption characteristics. Three LDVIs outperformed NDVI in estimating LAI, but not biomass. Multiple regression models were developed to improve the estimation of LAI and aboveground biomass of YST, and explained 75% and 53% of the variance in biomass and LAI, respectively, based on validation assessments with actual ground measurements.
Nomenclature: Yellow starthistle, *Centaurea solstitialis* L.
Key words: Invasive species, hyperspectral remote sensing, airborne hyperspectral data, vegetation index, biophysical estimation.

Yellow starthistle (YST) is a highly invasive exotic weed that is found throughout the western United States. It occurs primarily in agricultural rangelands, but also native grasslands, orchards, vineyards, pastures, roadsides, and wastelands. YST lowers yield and forage quality, reduces land value, and decreases water availability (Benefield et al. 2001; DiTomaso 2000; Harrod and Taylor 1995; Maddox 1981; Maddox et al. 1996). Control measures aimed at reducing YST populations have not been entirely successful. Better regional assessment and area-wide management techniques are needed to develop long-term sustainable management strategies to control YST (Carruthers 2003; DiTomaso et al. 2000).

Although traditional ground-based surveys can be used to assess and monitor invasive plants, surveys are labor intensive and have obvious limitations at landscape or larger scales due to high spatial variation of invasive plants and vast areas where such invasions occur (e.g., the California Department of Food and Agriculture now estimates that nine million ha of rangeland in the state is infested with YST). Studies have demonstrated that remote sensing can provide useful and reliable information on the infestation area and even detect the phenological stage of the target vegetation (Ge et al. 2006; Lass et al. 2005). Such information can be important for managers in assessing control options and as a warning tool for examining impacts of various invasive species (Anderson et al. 2005; Everitt et al. 1995, 1996; Ge et al. 2006; Lass et al. 2005).

DOI: 10.1614/WS-06-212.1
* First author, USDA—Agricultural Research Service, Exotic and Invasive Weeds Research Unit, 800 Buchanan St., Albany, CA 94710, and Earth and Planetary Sciences Department, University of California at Santa Cruz, 1156 High Street, Santa Cruz, CA 95064; second author, Center for Remote Sensing and Spatial Analysis, Department of Ecology, Evolution, and Natural Resources, Rutgers University, New Brunswick, NJ 08901; third author, USDA—Agricultural Research Service, Agriculture Research Systems Unit, 1500 N Central Ave. Sidney, MT 59270; fourth author, USDA—Agricultural Research Service, Exotic and Invasive Weeds Research Unit, 800 Buchanan St. Albany, CA 94710. Corresponding author's E-mail: shaokui@pw.usda.gov or gesk@nature.berkeley.edu

Previous research has explored the capability of using remote sensing to identify invasive plants and to estimate infestation coverage (Lass et al. 2005). Multispectral remote sensing with moderate spatial resolution, such as Landsat and SPOT imagery, has been used to detect the location of invasive species and to monitor the spread through time. However, because of the relatively coarse spatial and spectral resolution of SPOT and Landsat, these images have not been used successfully to identify and assess invasive herbaceous weeds (Everitt et al. 1995).

Airborne hyperspectral remote sensing offers an improved method to estimate important vegetation attributes at fine spatial resolutions (Bongers 2001; Cohen et al. 2002; Kerr and Ostrovsky 2003; Schmidtlein 2005; Turner et al. 2003; Vane and Goetz 1993). Hyperspectral remote-sensing data acquire imagery in many narrowly contiguous spectral bands and offer a more detailed view of the spectral properties from the ground targets than those data from the conventional multispectral bands, which are collected in a wide and sometimes noncontiguous band structure. However, because of the influences of environmental factors such as water content and nontarget vegetation in complex plant canopies, relationships between biological attributes and hyperspectral data are often masked and confounded by these factors (Blackburn 1998, 1999; Chappelle et al. 1992; Peñuelas et al. 1994). Therefore, it has been suggested that spectral data transformation using derivatives and pseudoabsorption, and the development of new vegetation indices, could aid in resolving these problems. Such techniques may minimize these influences and enhance relationships between important vegetation attributes and imaged data, especially in situations where only slight differences in vegetation cover are involved, as is often the case with invasive plant species (Blackburn 1998, 2002; Chen et al. 1998; Elvidge and Chen 1995; Peñuelas et al. 1994; Thenkabail et al. 2000; Tsai and Philpot 1998). Newly developed remote-sensing instruments and algorithms may allow more accurate vegetation detection and better characterization of specific habitat features, provide

better and more timely assessments, and improve area-wide vegetation management (Schmidtlein 2005).

Previous studies using airborne hyperspectral data have demonstrated that it can be used to identify YST over large areas (Lass et al. 1996, 2000, 2005). Hyperspectral remote sensing can also be used to monitor YST flowering phenology, which is important for assessment of biological control agent synchrony and potential impacts on the target weed (Ge et al. 2006). To date, however, there have been no studies that use hyperspectral remote-sensed data to estimate important biophysical attributes of this invasive weed, such as LAI and overall aboveground biomass. These biological attributes are important to both weed scientists and land managers interested in assessing YST infestation levels, population trends through time, and in developing or parametrizing population models and/or area-wide control strategies.

The objectives of this study were (1) to examine the correlations between hyperspectral vegetation indices and two important measurements of YST abundance, LAI and aboveground biomass; (2) to estimate actual LAI and biomass and compare on-the-ground measurements with the use of multiple vegetation indices derived from hyperspectral data; and (3) to combine these measures to assess the accuracy in using remote-sensed data to estimate LAI and aboveground biomass.

Materials and Methods

Study Area. A field study site was established along Bear Creek (122°22′56″W, 39°00′00″N), northwest of the city of Woodland in an area adjacent to and west of the Sacramento Valley of northern California, United States. In the summer of 2002, two ground-based data-collection plots were set up within this area to assess the use of hyperspectral data to develop estimation models of LAI and biomass. The plots were located in areas with nearly pure stands of YST (> 95% YST coverage). The only other plant material present in the plots was dry annual grass, which was not visible through the YST canopies. Within the study area, the field-measured LAI ranged from 0.04 to 2.33 (mean square error [MSE] was 0.11) and biomass (determined as aboveground dry weight) ranged from 50.42 to 71.27 g m^{-2} (MSE was 6.36).

Field Experimental Design and Data Collection. In late June 2002, two large 20-by-50–m modified Whittaker plots (MWP) were established within the study area. The Whittaker plot is designed for a multitiered vegetation sampling, and consists of 12 subplots strategically located within each plot. This sampling method has been modified to assess samples from the heterogeneous vegetation composed of diverse species combinations and/or varying densities of the target plant (Kalkhan and Stohlgren 2000; Stohlgren et al. 1995). In this study, we incorporated five additional 2-by-2-m^2 subplots in the middle of the standard MWP to increase the intensity of ground-based sampling (refer to Ge et al. 2006, Figure 2). In total, 34 subplots were established within the two MWPs. A full-range spectrometer[1] was used to measure canopy reflectance randomly at approximately 20 cm above the canopy within each subplot. The spectrometer probe acquired data across a field of view of 25° and provided a representative sample covering 61.73 cm^2 within each subplot. The number of spectral measurements in a subplot was approximately 10 times the root square of the subplot area (i.e., $N \approx 10 * \sqrt{area_{\text{subplot}}}$). In addition, supplemental reflectance measurements were collected over an asphalt road and bare soil at 20 locations within 100 m of the two MWPs. These reflectance curves were used to help calibrate the airborne hyperspectral imagery collected by a Compact Airborne Spectrographic imaging system-II (CASI-II).[2]

LAI was measured on the ground with the use of a plant canopy analyzer (PCA)[3] on the same day as the spectral data were collected with the CASI-II. Aboveground biomass of YST was measured within 3 d of the CASI-II flyover from each of the 34 subplots with the use of 0.5-by-0.5–m quadrat samples. All aboveground YST tissue in the quadrats was harvested, bagged, and returned to the lab for processing. Each biomass sample was individually weighed in the lab, oven dried at 70 C for 72 h, and then weighed again to acquire dry-weight biomass and the water content at harvest.

Hyperspectral images were acquired by the CASI-II on June 30, 2002. At-sensor digital data were collected across 48 wavelength bands within a spectral range of 426.7 to 965.1 nm. Bandwidths ranged from 11.2 to 12.6 nm. The images were taken at approximately 1,500 m above the ground, resulting in a spatial resolution of 2 m per pixel. In conjunction with the CASI-II image collection, high-reflectance corner markers were deployed 4 m away from the vertices of each MWP. These markers were used to aid in image rectification and plot boundary identification. A global positioning system (GPS)[4] with submeter accuracy was used to measure the geographic coordinates of the plots and subplots, allowing accurate determinations of the specific locations of YST samples within each MWP. Additionally, submeter-resolution GPS points were collected for all the soil and asphalt sampling locations to correspond with reflectance values collected over these sites.

Image Processing and Analysis. The ground-based reflectance curves acquired by the spectrometer over each MWP subplot were averaged to obtain a canopy reflectance (R) curve for each individual subplot. These 34 averaged reflectance values, along with the 40 reflectance values collected from over the asphalt-road and bare-soil areas, were further processed to match the CASI-II bandwidths. This was accomplished by merging the original ground-based spectral data through a mean function (i.e., $R_{CB} = \left[\sum_{i=1}^{n} R_{SB}/n\right]$), resulting in convoluted reflectance values for CASI-II bands from the ground reflectance as measured by the spectrometer. R_{SB} are reflectance values of the spectrometer covered by the matching CASI-II band and n is the number of the corresponding bands of spectrometer covered by the respective CASI-II band. CASI-II data used in this study cover only the visible and the near-infrared (NIR) regions of the spectrum, from 450 to 975 nm; therefore, only the reflectance data from the ground-based spectrometer that matched these CASI-II bands were used in this analysis. In order to convert the raw hyperspectral images to surface reflectance values, empirical models (Ben-Dor et al. 1994; Ben-Dor and Levin 2000) were developed for each CASI-II band by regressing CASI-II digital data with the corresponding convoluted spectral data of the different ground targets (including YST, bare soil, and asphalt). The CASI-II data (geographically tagged and spectrally adjusted

pixels) representing the sampled YST plots and subplots were extracted from the data set based on their locations measured with the submeter GPS unit. With the use of these extracted surface reflectance values from the selected areas, spectral derivatives and two categories of vegetation indices (i.e., derivative-based normalized difference [DNDVI] and local derivative vegetation indices [LDVI]) were calculated. The correlations between these derivatives and vegetation indices and the measured vegetation variables (LAI and aboveground biomass) were assessed. These derivatives and vegetation indices were calculated as follows:

Derivatives Based on Hyperspectral Images. Two types of derivatives have been developed with hyperspectral reflectance (Blackburn 1998; Yoder and Pettigrew-Crosby 1995):

$$DR_i = (R_{i+1} - R_{i-1})/\mathrm{BW} \quad [1]$$

$$DLR_i = (\mathrm{Log}[1/R_{i+1}] - \mathrm{Log}[1/R_{i-1}])/\mathrm{BW} \quad [2]$$

where DR_i and DLR_i are the derivatives at the ith band from the reflectance and pseudoabsorption spectra, R_{i+1} and R_{i-1} are the reflectance values of the $(i + 1)$ and $(i - 1)$ CASI-II bands, respectively, and BW is the bandwidth. The Pearson coefficients of correlation were used to determine derivatives of which CASI-II bands could be used to estimate LAI and biomass.

Derivative-Based Normalized Difference Vegetation Indices (DNDVI). These measures are similar to the broadband NDVI that is often used in vegetation assessment with multispectral images. In this case, DNDVIs were calculated based on two derivatives, one from the reflectance and one from the pseudoabsorption (reciprocal of reflectance) data for each of the visible bands of interest (blue, green, and red bands). In total, six different estimators of DNDVI were produced as follows:

$$\mathrm{DNDVIR}_b = \frac{DR_{\mathrm{NIR}} - DR_b}{DR_{\mathrm{NIR}} + DR_b} \quad [3]$$

$$\mathrm{DNDVIP}_b = \frac{PDR_{\mathrm{NIR}} - PDR_b}{PDR_{\mathrm{NIR}} + PDR_b} \quad [4]$$

$$\mathrm{NDVIRR}_g = \frac{DR_{\mathrm{NIR}} - DR_g}{DR_{\mathrm{NIR}} + DR_g} \quad [5]$$

$$\mathrm{DNDVIP}_g = \frac{PDR_{\mathrm{NIR}} - PDR_g}{PDR_{\mathrm{NIR}} + PDR_g} \quad [6]$$

$$\mathrm{DNDVIR}_r = \frac{DR_{\mathrm{NIR}} - DR_r}{DR_{\mathrm{NIR}} + DR_r} \quad [7]$$

$$\mathrm{DNDVIP}_r = \frac{PDR_{\mathrm{NIR}} - PDR_r}{PDR_{\mathrm{NIR}} + PDR_r} \quad [8]$$

where DNDVIR and DNDVIP are individual vegetation indices developed by assessing the derivatives of reflectance and pseudoabsorption, respectively. The subscripts *b*, *g*, and *r* indicate that the derivative used to develop the vegetation index is selected from one of three visible spectral regions (i.e., blue, green, and red narrow bands, respectively) and that this selected derivative is most highly correlated with LAI and biomass, compared with derivatives of any other neighboring wavelengths within the blue, green, and red regions. Similarly, the selected derivatives of the near-infrared bands are also highly correlated with LAI and aboveground biomass in the NIR plateau.

Traditional NDVI values were also estimated with the use of the narrowband hyperspectral data. These were compared with the derivative-based vegetation indices and used to assess correlations with YST LAI and biomass. In general, the red and near-infrared bands used to estimate NDVI were chosen from the red absorption peak around 670 to 680 nm and the near-infrared plateau around 800 nm. In this study, the corresponding bands centered specifically at 675.7 and 802.4 nm.

$$\mathrm{NDVI} = \frac{R_{802.4} - R_{675.7}}{R_{802.4} + R_{675.7}} \quad [9]$$

The Local First-Order Derivative-Based Vegetation Indices (LDVI). The first-order hyperspectral-based derivatives were integrated along the slope of the red edge. The red edge is located between the red and the near-infrared regions, and reflectance of vegetation changes rapidly within this defining spectral range. Estimates of these parameters have previously been used to quantify green vegetative cover (Chen et al. 1998; Thenkabail et al. 2000). In this study, these derivatives were modified to integrate the local absorption and reflectance trends along the slopes of both the blue and red absorption features and also to assess plant reflectance characteristics to enhance the spectral patterns associated with YST LAI and biomass. In order to differentiate these indices from the normalized vegetation indices, we considered them as ''local'' derivative vegetation indices, which were calculated as:

$$\mathrm{LDVIR} = \left(\sum_{\lambda_1}^{\lambda_n} [DR_\lambda - DR_r] * \mathrm{BW}_i\right) \Big/ \sum_{\lambda_1}^{\lambda_n} \mathrm{BW}_i \quad [10]$$

$$\mathrm{LDVIP} = \left(\sum_{\lambda_1}^{\lambda_n} [PDR_\lambda - PDR_r] * \mathrm{BW}_i\right) \Big/ \sum_{\lambda_1}^{\lambda_n} \mathrm{BW}_i \quad [11]$$

where LDVIR and LDVIP are the first-order derivative vegetation indices calculated from reflectance and pseudoabsorption, respectively. BW_i is the bandwidth from band λ_1 (where the positive slope began) to band λ_n (where the slope ended). DR_r and PDR_r are defined as the referenced derivatives of reflectance and pseudoabsorption at the targeted bands, which were the local minimum derivative values along the slope of absorption or reflectance. The minimum values for each parameter were determined from the spectra, averaged over the data collected from all 34 MWP subplots. These minimums were considered local baselines from which the derivatives were integrated along the subsequent slopes. Such indices captured local magnitudes of reflectance or absorption relative to the nearest reference reflectance peak or absorption center. In other words, they characterized the fine differences in each of the measured spectral patterns rather than the general band ratios, as is done in NDVI.

The position of the referred minimum derivative was 460.2 nm for the blue band. Within the blue wavelength

region, the corresponding LDVI was calculated from the spectral range of 460.2 to 493.9 nm, which was the area of most importance in the blue absorption portion of the spectra. Within the green bands (550.3 to 573.0 nm), the local referenced position was 550.3 nm, which was at the point of peak reflectance caused by the plant green tissues. Within the red absorption area (641.3 to 675.7 nm), LDVI was integrated with the use of a referenced derivative at 641.3 nm, which corresponded to an intense absorption by chlorophyll.

Model Development. After calculating the derivatives (i.e., LDVIRs, LDVIPs, and LDVIs), their relationships to ground-measured YST biomass and LAI were examined by testing for significant correlation coefficients between the remote-sensed and field-measured data. In order to reduce the colinearity of the spectral data, a subset of the sample variables were first selected with the use of Mallow's C_p to develop a best-fit model (Selvin 1998).

$$C_p = \sum_{i=1}^{p} (y - y_p)^2 \Big/ s^2 - n + 2p \qquad [12]$$

In this equation, y_p is the predicted value of y from p independent spectral indices that are correlated with YST LAI and biomass. The parameter s^2 is the mean-square error (MSE) of the regression, and n is the sample size. By minimizing C_p, the best subsets were selected from the complete set of spectral variables that originally showed significant correlation with YST LAI and biomass. The selected subsets were then used to develop models with the use of a cross-validation method (Venter and Snyman 1995). To accomplish this, the 34 subplot samples were randomly divided into seven groups. The model was then independently derived seven different times. Each time, six groups were used as training data to calibrate models for estimating LAI and biomass. The seventh group was used as an independent test group to validate the models. The model from which the error was closest to the average error from the seven iterations was selected as the best predictor. This process was implemented with the use of the following function:

$$y = f_i(x_i) + \varepsilon \qquad [13]$$

where y is the predicted value estimated by the model using the training groups, x_i is one of the selected training variables, and f is the corresponding linear function. The parameter ε represents the model error, indicating the difference between the estimated values and the actual field-collected test data.

Results and Discussion

Correlations Between Hyperspectral Derivatives and Vegetation Attributes. Hyperspectral derivatives improved the relationships between remotely sensed spectral data and LAI and biomass. Derivatives of reflectance performed better at estimating LAI and biomass than derivatives of pseudoabsorption, although they both had high correlation coefficients. The best single-band derivatives explained 50% and 56% of the variance of LAI and biomass, respectively (Figure 1). The original reflectance data were poorly correlated with LAI ($r < 0.50$, $P > 0.05$); however, the derivatives within the blue (at 483 nm) and red (at 653 and 664 nm) spectral regions were correlated ($r = 0.52$, 0.71, and 0.59, respectively). Similarly, derivatives of reflectance also enhanced the correlations with LAI within the range of NIR bands, where the values of 10 bands, from 774.6 to 848.8 nm, were also correlated with LAI ($r = 0.60$ and 0.69, $n = 34$, $P < 0.01$). It was found that derivatives of pseudoabsorption of four bands (one in the blue region, two in the red region, and one in the NIR region) were correlated with LAI ($r = 0.50$ to 0.60, $P < 0.01$). Based on correlation analyses, we found that hyperspectral derivatives were better than the original reflectance data in estimating LAI.

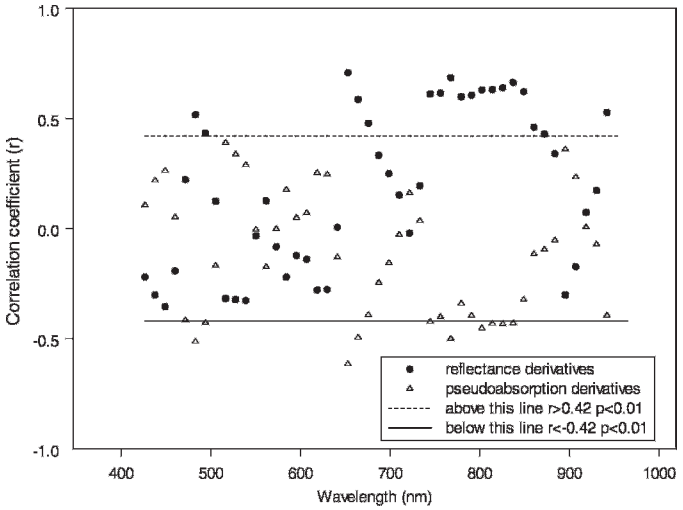

Figure 1. Correlation between derivative-based reflectance (DR) and pseudoabsorption (PDR) and LAI of yellow starthistle.

Derivative transformations also enhanced the ability of hyperspectral CASI-II data to estimate the aboveground biomass of YST. There were high correlations between derivatives and biomass at a few visible wave bands ($r = 0.52$ to 0.65, $P < 0.01$, Figure 2). Compared with the derivatives of reflectance, the derivatives of pseudoabsorption were better correlated with biomass in the blue region. The blue wave bands were located at 471.5, 482.7, and 493.9 nm ($r = -0.64$, -0.75, and -0.71, respectively). Similarly, the pseudoabsorption derivatives through most of the NIR bands had strong correlations with biomass ($r = 0.54$ to 0.67).

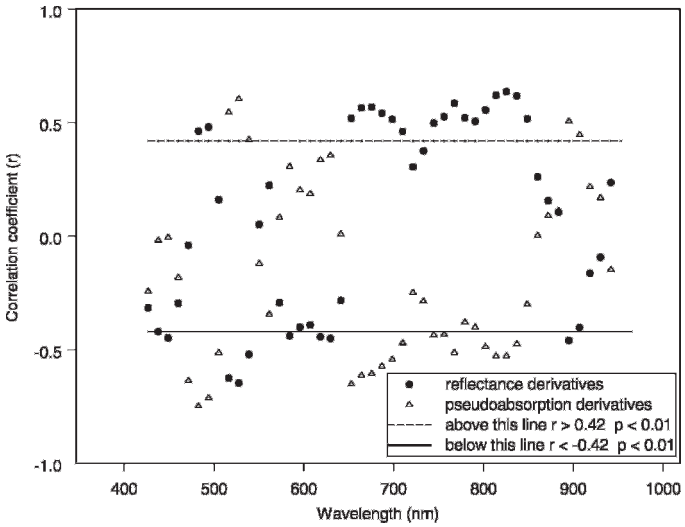

Figure 2. Correlation between derivative-based reflectance (DR) and pseudoabsorption (PDR) and biomass of yellow starthistle.

Table 1. Correlations between the derivative-based normalized vegetation indices (DNDVI) and LAI and biomass.

Biophysical parameters	DNBR[a]	DNBP[b]	DNGR[a]	DNGP[b]	DNRR[a]	DNRP[b]	NDVI[c]
LAI	0.40	0.00	0.39	0.42	0.37	− 0.48	0.43
Biomass	0.72	0.32	0.72	0.71	0.60	− 0.53	0.64

[a] DNBR, DNGR, and DNRR are derivative-based normalized difference vegetation indices that normalized reflectance derivatives of the chosen blue, green, and red bands by the reflectance derivatives of the chosen NIR band, respectively.
[b] DNBP, DNGP, and DNRP are derivative-based normalized difference vegetation indices that normalized pseudoabsorption derivatives of the chosen green spectral bands by the pseudoabsorption of the chosen NIR band.
[c] NDVI was developed by using a hyperspectral red band centered at 675.70 nm normalized by a NIR band centered at 802.40 nm.

Although the CASI-II imagery had both high spectral and high spatial resolutions, YST LAI and biomass were not correlated with the original spectra data. However, by derivative transformations, correlations between spectral data and the ground-based LAI and biomass were improved. For individual narrow bands, the highest correlation coefficients of derivatives approached 0.71, which was much better than the correlations obtained using the original reflectance data. It is further noted that the derivative estimators performed better in the blue and red regions, presumably due to plant pigments that enhanced absorption characteristics in these spectral wavelengths (Blackburn 1998, 1999).

The derivatives of hyperspectral data have been widely used to assess and estimate a variety of important vegetation parameters, such as total chlorophyll, chlorophyll b, and carotenoids of plants (Blackburn and Steele 1999). Although some of these derivatives have very high correlations with key biophysical attributes of plants, the correlation depends upon the spectral wavelengths and biophysical variables under study. As in our situation, these correlative spectral wave bands are usually located in the blue and red absorption ranges. Therefore, spectral derivatives not only minimize the influences of external factors but also emphasize the spectral effects of key plant components (Blackburn and Steele 1999; Serrano et al. 2002).

Correlations Between Derivative-Based Vegetation Indices and LAI /Biomass. Correlation coefficients between NDVI and YST LAI and biomass were 0.43 and 0.64, respectively (Table 1). Three DNDVI functions performed better in estimating biomass of YST than commonly used NDVI. These indices showed improved correlation with aboveground biomass ($r = 0.71$ to 0.72, $P < 0.001$). However, DNDVI did not improve the relationship with LAI. DVBP, DVGP, and DVRR showed better correlation with LAI than NDVI; their correlation coefficients were 0.59, 0.47, and − 0.66, respectively (Table 2).

A previous case study demonstrated that hyperspectral-based vegetation indices calculated from derivatives improved the relationship between spectral data and vegetation attributes. The first-order derivative green vegetation index was strongly correlated with LAI of pinyon pines near Reno, NV, having R^2 values of 0.94. The derivative-based vegetation index strongly improved the relationship between the spectral data and LAI (Elvidge and Chen 1995). In this study, hyperspectral vegetation indices developed from spectral derivatives improved estimation of LAI and aboveground biomass of YST from hyperspectral remotely sensed data. Compared with the study case of pinyon pines, the derivative-based indices did not have as strong a relationship with YST LAI and biomass. However, this exploratory study has made progress in using hyperspectral data to assess and monitor species-level invasive plants, following previous applications of using hyperspectral data to detect the presence of invasive weeds, such as YST and spotted knapweed (*Centaurea maculosa* Lam.) (Lass et al. 2005).

Modeling LAI and Aboveground Biomass. Although LAI was correlated with 15 different indices calculated from the CASI-II data, only five of the LDVIs and DNDVIs were selected to develop a multiple estimation model. Wave bands of these five variables were located from the red to the NIR regions. All five variables were derivatives of reflectance values, as no derivatives of pseudoabsorption or any other vegetation index were used in the final model. This further confirmed that derivatives of reflectance outperformed both pseudoabsorption-based vegetation indices and derivatives in estimating YST LAI.

Similarly, we found that five spectral-derived variables were selected in the model to estimate biomass of YST. Two of the variables were reflectance-based derivatives in the NIR bands, two were normalized reflectance-derived vegetation indices, and one was from the pseudoabsorption-based LDVI. All the variables and their corresponding coefficients that were used in the final models to estimate LAI and biomass are summarized in Table 3. When comparing P values, it was found that the reflectance-based derivative at 652.8 nm was more significant than any of the other selected predictors to estimate LAI; and that the NDGR and DVBP performed better in estimating the aboveground biomass of YST than any of other three variables in the biomass estimation model.

Through the validation process using field-measured data, it was found that CASI-II data could be used to estimate LAI and aboveground biomass of YST remotely. The final

Table 2. Correlations between the local integrative derivatives vegetation indices (LDVI) and LAI and biomass.

Biophysical parameters	DVBR[a]	DVBP[b]	DVGR[a]	DVGP[b]	DVRR[a]	DVRP[b]
LAI	−0.25	0.59	− 0.22	0.47	− 0.66	− 0.10
Biomass	−0.40	0.68	− 0.28	0.60	− 0.57	− 0.44

[a] DVBR, DVGR, and DVRR were the first-order derivative-based local vegetation indices developed by the reflectance derivatives in the blue, green, and red regions, respectively.
[b] DVBP, DVGP, and DVRP are the first-order derivative-based local vegetation indices developed by the pseudoabsorption derivatives in the blue, green, and red regions, respectively.

Table 3. The selected variables in the calibration models to estimate LAI and aboveground biomass of yellow starthistle.

Estimated parameters	Variables	Coefficient	P value
LAI	Intercept	− 0.45	0.03
	DR652.8	$3.35*10^3$	< 0.01
	DR744.6	$-7.04*10^3$	0.02
	DR767.7	$9.52*10^3$	0.02
	DR814.0	$-2.01*10^4$	0.04
	DR825.6	$1.99*10^4$	0.01
	RMSE: 0.28	Model's R^2	0.76
Biomass	Intercept	$-2.83*10^2$	< 0.01
	DR814.0[a]	$-8.25*10^5$	0.02
	DR837.2		0.03
	DNGR[b]	$1.47.75*10^5 4*10^3$	< 0.01
	DNRR[b]	$-9.04*10^2$	0.02
	DVBP[b]	$9.09*10^4$	0.01
	RMSE: 19.44	Model's R^2	0.86

[a] DRXXX stood for the derivative of reflectance at the position of XXX (nm) wavelength.
[b] DNGR, DNRR, and DVBP are the same as in Tables 1 and 2.

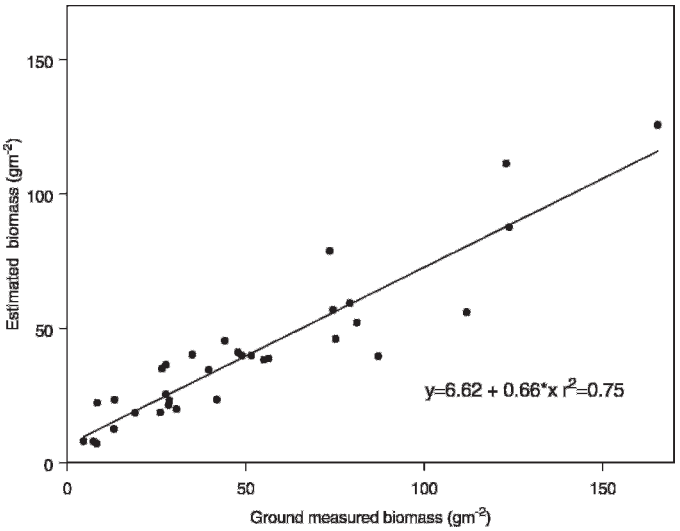

Figure 4. Comparison between the estimated and field-measured values of biomass of yellow starthistle.

estimation models explained 53% and 75% of the variance in LAI and biomass, respectively (Figures 3 and 4). The multiple-variable models had better estimation than any single spectral band.

Although estimation models of LAI and biomass were both determined to be significant, the LAI model explained 53% of the LAI ground-measured variance. When the estimated and ground-measured LAI values were compared, it was found that errors of LAI estimation were not related to LAI levels (Figure 3). The error may have been caused by leaf shape and canopy architecture of YST. At the time of the year when this imaging was conducted, the individual patch of YST had a very open canopy structure and bolting plants often lacked significant leaf structure. The uncertainty of LAI estimation most likely resulted from small and irregular leaf shapes, in a canopy with just a few round and narrow leaves growing on the dense green branches. However, biomass estimation revealed that hyperspectral derivative-based vegetation indices are superior to a traditional vegetation index, NDVI.

Although some single-band spectral data and vegetation indices often have strong relationships with important biophysical factors of plants, it is not always possible to use an individual spectral variable to estimate these attributes accurately with the use of remote-sensed data. Therefore, multivariate analysis is often used to select the optimal spectral variables needed to develop accurate predictive models (Cohen et al. 2002). Biological parameters may be correlated with multiple narrowband spectral data and derived vegetation indices, due to underlying spectral characteristics associated with plant components such as pigment and water absorption. Therefore, to increase the estimation accuracies of vegetation characteristics, such as LAI and biomass, it is important to develop multiple-variable models by selecting the best subset of spectral-based variables to avoid unnecessary cross-correlation and colinearity.

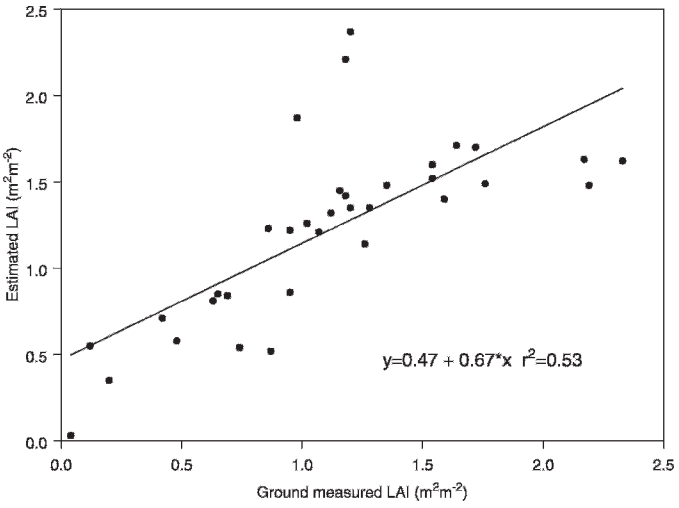

Figure 3. Comparison between the estimated and field-measured values of LAI of yellow starthistle.

Previous studies have shown that hyperspectral images can be used to identify YST from surrounding vegetation (Lass et al. 1996) and to assess its phenological stages (Ge et al. 2006). This study demonstrated that the estimation of LAI and biomass derived from hyperspectral imagery is feasible, although there are still limitations in assessment that need to be overcome, and improvements made in both the timing of application and analysis of the acquired data in order to apply this research readily to field management. Because this was a single-year study conducted at a specific time, it will be important to note that this study was done only in 1 year. It will be important to replicate this study to verify these results and to determine the robustness of derivative-based indices. With further improvements in both equipment and methodology, these new tools may become an important component of an integrated weed monitoring and management program. This approach to estimating LAI and biomass may be a step in developing a more effective and efficient method of acquiring such biological attribute data over wide areas. When successful, the resulting estimates may be extended via interpolation and extrapolation to unsampled ground locations where imagery is available. Such estimation can then be used to map predicted YST distributions in space and time, and may improve our understanding of key physical and chemical attributes important for vegetation growth and management (Borge and Leblanc 2000; Sims and Gamon 2002; Strachan et al. 2002). The use of spatially explicit models to quantify the

growth and abundance of plants over a large area and to evaluate long-term sustainable control strategies may be possible in the future and deserves further evaluation (Collingham et al. 1997, 2000; Wadsworth et al. 2000).

Sources of Materials

[1] FieldSpec@ 3 (350 to 2,500 nm) Analytical Spectral Device (ASD), Inc., 5335 Sterling Drive, Suite A, Boulder, CO 80301.

[2] CASI-II VNIR spectrographic imaging system, ITRES Research Limited, No. 110, 3553, 31st Street N.W., Calgary, Alberta T2L2K7, Canada.

[3] LI-COR LAI-2000, LI-COR Environmental, 4647 Superior Street, P.O. box 4425, Lincoln, NE 68504.

[4] The GeoXTTM high-performance submeter GPS receiver, Trimble, 935 Stewart Drive, Sunnyvale, CA 94085.

Acknowledgments

We thank Dr. Le Wang, Dr. Jun Yang, Dr. Qi Chen, and Dr. Desheng Liu for field assistance. We also appreciate the assistance of Dr. Peng Gong and Dr. Ruiliang Pu for advice on field sampling and experimental design. In particular, we are grateful to two anonymous reviewers and Dr. Richard G. Smith for their constructive comments on revisions of the manuscript. This project was partially supported by the USDA Agricultural Research Service (Project No. 5325-22000-020-00D), the USDA Cooperative State Research Education and Extension Service (Project No. 00-52103-9647), and NASA Earth Science Invasive Species Application (Project No. N06-4918).

Literature Cited

Anderson, G. L., R. I. Carruthers, S. Ge, and P. Gong. 2005. Cover: monitoring of invasive *Tamarix* distribution and effects of biological control with airborne hyperspectral remote sensing. Int. J. Remote Sens. 26:2487–2489.

Ben-Dor, E., F. A. Kruse, and A. Banin. 1994. Comparison of three calibration techniques for utilization of GER 63-channel aircraft scanner data of Makhtesh Ramon, Negev, Israel. Photogram. Eng. Remote Sens. 60:1339–1354.

Ben-Dor, E. and E. Levin. 2000. Determination of surface from raw hyperspectral data without simultaneous ground data measurements, a case study of the GER 63-channel sensor data acquired over Naan, Israel. Int. J. Remote Sens. 10:2053–2074.

Benefield, C. B., J. M. DiTomaso, G. B. Kyser, and A. Tschohl. 2001. Reproductive biology of yellow starthistle (*Centaurea solstitialis*): maximizing late season control. Weed Sci. 49:38–90.

Blackburn, G. A. 1998. Quantifying chlorophylls and carotenoids at leaf and canopy scales: an evaluation of some hyperspectral approaches. Remote Sens. Environ. 66:273–285.

Blackburn, G. A. 1999. Relationships between spectral reflectance and pigment concentrations in stacks of deciduous broadleaves. Remote Sens. Environ. 70:224–237.

Blackburn, G. A. 2002. Remote sensing of forest pigments using airborne imaging spectrometer and LIDAR imagery. Remote Sens. Environ. 82:311–321.

Blackburn, G. A. and C. M. Steele. 1999. Towards the remote sensing of matorral vegetation physiology—adaptation and acclimation mechanisms. Remote Sens. Environ. 70:278–292.

Bongers, F. 2001. Methods to assess tropical rain forest canopy structure: an overview. Plant Ecol. 153:263–277.

Borge, N. H. and E. Leblanc. 2000. Comparing prediction power and stability of broadband and hyperspectral vegetation indices for estimation of green leaf area index and canopy chlorophyll density. Remote Sens. Environ. 76:156–172.

Carruthers, R. I. 2003. Invasive species research in the USDA Agriculture Research Service. Pest Manag. Sci. 59:827–834.

Chappelle, E. W., M. S. Kim, and J.E.I. McMurtrey. 1992. Ratio analysis of reflectance spectra (RARS): an algorithm for the remote estimation of the concentrations of chlorophyll a, chlorophyll b, and carotenoids in soybean leaves. Remote Sens. Environ. 39:239–247.

Chen, Z., C. D. Elvidge, and D. P. Groeneveld. 1998. Monitoring seasonal dynamics of arid land vegetation using AVIRIS data. Remote Sens. Environ. 65:255–266.

Cohen, W. B., T. K. Maiersperger, S. T. Gower, and D. P. Turner. 2002. An improved strategy for regression of biophysical variables and Landsat ETM+ data. Remote Sens. Environ. 58:1–11.

Collingham, Y. C., M. O. Hill, and P. E. Hulme. 1997. The use of a spatially explicit model to simulate the spread of riparian weeds. Pages 45–52 *in* A. Cooper and J. Power, eds. Proceedings of the International Association for Landscape Ecology: Species Dispersal and Land Use Processes. Belfast: IALE.

Collingham, Y. C., R. A. Wadsworth, B. Huntley, and P. E. Hulme. 2000. Predicting the spatial distribution of alien riparian species; issues of spatial scale. J. Appl. Ecol. 37(Suppl. 1):13–27.

DiTomaso, J. M. 2000. Invasive weeds in rangelands: species, impacts and management. Weed Sci. 48:255–265.

DiTomaso, J. M., G. B. Kyser, S. B. Orloff, and S. F. Enloe. 2000. Integrated approaches and control option considerations when developing a management strategy for yellow starthistle. Calif. Agric. 54:30–36.

Elvidge, C. D. and Z. Chen. 1995. Comparison of broad-band and narrow-band red and near-infrared vegetation indexes. Remote Sens. Environ. 54:38–48.

Everitt, J. H., D. E. Escobar, M. A. Alaniz, M. R. Davis, and J. V. Richerson. 1996. Using spatial information technologies to map Chinese tamarisk (*Tamarix chinensis*) infestations. Weed Sci. 44:194–201.

Everitt, J. H., D. E. Escobar, and M. R. Davis. 1995. Using remote sensing for detecting and mapping noxious plants. Weed Abstr. 44:639–649 .

Ge, S., J. H. Everitt, R. I. Carruthers, P. Gong, and G. Anderson. 2006. Hyperspectral characteristics of canopy components and structure for phenological assessment of an invasive weed. Environ. Monit. Assess. 120:109–126.

Harrod, R. J. and R. J. Taylor. 1995. Reproduction and pollination biology of *Centaurea* and *Acroptilon* species, with emphasis on *C. diffusa*. Northwest Sci. 69:97–105.

Kalkhan, M. A. and T. J. Stohlgren. 2000. Using multi-scale sampling and spatial cross-correlation to investigate patterns of plant species richness. Environ. Monit. Assess. 64:591–605.

Kerr, J. T. and M. Ostrovsky. 2003. From space to species: ecological applications for remote sensing. Trends Ecol. Evol. 18:299–305.

Lass, L. W., H. W. Carson, and R. H. Calihan. 1996. Detection of yellow starthistle (*Centaurea solstitialis*) and common St. Johnswort (*Hypericum perforatum*) with multispectral digital imagery. Weed Technol. 10:466–474.

Lass, L. W., T. S. Prather, N. F. Glenn, K. T. Weber, J. T. Mundt, and J. Pettingill. 2005. A review of remote sensing of invasive weeds and example of the early detection of spotted knapweed (*Centaurea maculosa*) and babysbreath (*Gypsophila paniculata*) with a hyperspectral sensor. Weed Sci. 53:242–251.

Lass, L. W., B. Shafii, W. J. Price, and D. C. Thill. 2000. Assessing agreement in multispectral images of yellow starthistle (*Centaurea solstitialis*) with ground truth data using a Bayesian methodology. Weed Technol. 14:539–544.

Maddox, D. M. 1981. Introduction, Phenology, and Density of Yellow Starthistle in Coastal, Intercoastal, and Central Valley Situations in California. Washington, DC: U.S. Department of Agriculture (USDA) ARS Rep. ARR-W-20. Pages 1–33.

Maddox, D. M., D. B. Joley, D. M Supkoff, and A. Mayfield. 1996. Pollination biology of yellow starthistle (*Centaurea solstitialis*) in California. Can. J. Bot. 74:262–267.

Peñuelas, J., J. A. Gammon, A. L. Fredeen, J. Merino, and C. B. Field. 1994. Reflectance indices associated with physiological changes in nitrogen- and water-limited sunflower leaves. Remote Sens. Environ. 48:135–146.

Schmidtlein, S. 2005. Imaging spectroscopy as a tool for mapping Ellenberg indicator values. J. Appl. Ecol. 42:966–974.

Selvin, S. 1998. Modern applied biostatistical methods: using S-plus. Oxford, UK: Oxford University Press. 461 p.

Serrano, L., J. Peñuelas, and S. L. Ustin. 2002. Remote sensing of nitrogen and lignin in Mediterranean vegetation from AVIRIS data: decomposing biochemical from structural signals. Remote Sens. Environ. 81:355–364.

Sims, D. A. and J. A. Gamon. 2002. Relationships between leaf pigment content and spectral reflectance across a wide range of species, leaf structures and development stages. Remote Sens. Environ. 81:337–354.

Stohlgren, T. J., M. B. Falkner, and L. D. Schell. 1995. A modified-Whittaker nested vegetation sampling method. Vegetatio 117:113–121.

Strachan, I. B., E. Pattey, and J. B. Boisvert. 2002. Impact of nitrogen and environmental conditions on corn as detected by hyperspectral reflectance. Remote Sens. Environ. 80:213–224.

Thenkabail, P. S., R. B. Smith, and E. De-Pauw. 2000. Hyperspectral vegetation indices for determining agricultural crop characteristics. Remote Sens. Environ. 71:158–182.

Tsai, F. and W. Philpot. 1998. Derivative analysis of hyperspectral data. Remote Sens. Environ. 66:41–51.
Turner, W., S. Spector, N. Gardiner, M. Fladeland, E. Sterling, and M. Steininger. 2003. Remote sensing for biodiversity science and conservation. Trends Ecol. Evol. 18:306–314.
Vane, G. and A.F.H. Goetz. 1993. Terrestrial images spectrometry: current status, future trends. Remote Sens. Environ. 44:117–126.
Venter, J. H. and J.L.J. Snyman. 1995. A note on the generalized cross-validation criterion in linear model selection. Biometrika 82:215–219.
Wadsworth, R. A., Y. C. Collingham, S. G. Willis, B. Huntley, and P. E Hulme. 2000. Simulating the spread and management of alien riparian weeds: are they out of control? J. Appl. Ecol. 37(Suppl. 1):28–38.
Yoder, B. J. and R. E. Pettigrew-Crosby. 1995. Predicting nitrogen and chlorophyll content and concentrations from reflectance spectra (400–2500 nm) at leaf and canopy scales. Remote Sens. Environ. 53:199–211.

Received December 15, 2006, and approved July 12, 2007.